

# Production and propagation of secondary antideuteron in the Galaxy

Luis Fernando Galicia Cruztitla<sup>†</sup> and Diego Mauricio Gómez Coral<sup>\*</sup>

Instituto de Física, Universidad Nacional Autónoma de México, Circuito de la Investigación Científica, Ciudad Universitaria, CDMX, 04510, Mexico

<sup>\*</sup> [dgomezco@fisica.unam.mx](mailto:dgomezco@fisica.unam.mx), <sup>†</sup> [luisfergac@ciencias.unam.mx](mailto:luisfergac@ciencias.unam.mx)



22nd International Symposium on Very High Energy Cosmic Ray Interactions (ISVHECRI 2024)  
Puerto Vallarta, Mexico, 8-12 July 2024  
doi:[10.21468/SciPostPhysProc.?](https://doi.org/10.21468/SciPostPhysProc.)

## Abstract

This work reviews the current state of the antideuteron ( $\bar{d}$ ) production cross-sections in cosmic ray interactions and its uncertainties, considering the coalescence model and measurements in accelerator experiments. These cross-sections have been included in a simulation of cosmic rays propagation in the Galaxy using GALPROP v.57, with updated parameters of the diffusive reacceleration model. An estimation of the expected antideuteron flux at Earth is presented.

Copyright attribution to authors.

This work is a submission to SciPost Phys. Proc.

License information to appear upon publication.

Publication information to appear upon publication.

Received Date

Accepted Date

Published Date

1

## 2 Contents

3	<b>1 Introduction</b>	<b>2</b>
4	<b>2 Transport of galactic CRs</b>	<b>2</b>
5	<b>3 Secondary antideuteron production</b>	<b>3</b>
6	3.1 Coalescence model	3
7	3.2 Secondary source term	3
8	<b>4 Results</b>	<b>4</b>
9	4.1 Differential cross section production and source term for $\bar{d}$	4
10	4.2 Expected $\bar{d}$ flux	4
11	<b>5 Conclusion</b>	<b>5</b>
12	<b>References</b>	<b>5</b>

13

14

## 1 Introduction

Cosmic Rays (**CRs**) produced in stars and accelerated into the Interstellar Medium (**ISM**) in supernova remnants (**SNRs**) are called *primary cosmic rays*. Composed mostly of protons (p) and Helium (He), these primary particles interact with the **ISM** through inelastic collisions producing *secondary cosmic rays* [1]. In a Universe dominated by matter, and within the Standard Model of particles (**SM**), the production of antimatter could only be possible through the nuclear interactions of **CRs** with the **ISM**, i.e. antimatter is expected to be of *secondary* origin. However, Dark Matter (**DM**) models predict  $\bar{d}$  production by annihilation or decay of **DM** particles in the Galaxy [2]. This additional primary  $\bar{d}$  production would be observed as an excess to the secondary component at energies below 1 GeV [3]. Interestingly, the Alpha Magnetic Spectrometer (AMS-02) detector onboard the International Space Station (**ISS**) has reported 7  $\bar{d}$  candidates in the energy region above 1 GeV [4]. Although a **DM** origin of these  $\bar{d}$  seems to be in tension with the observations, a clear interpretation of the results requires a good estimation of the secondary component. Therefore, in this work a review of the  $\bar{d}$  production cross sections within the coalescence model, and an estimation of the flux after propagation in the Galaxy are presented.

## 2 Transport of galactic CRs

Charged **CRs** particles propagate in the Galaxy following a diffusive process due to perturbations in the magnitude and direction of the magnetic fields of the different regions of the Galaxy. As a consequence, **CRs** confined time in the galactic volume is on the order of megayears [5]. The dynamics of the propagation of **CRs** in the Galaxy is modeled by the *transport equation* [6]:

$$\frac{\partial \psi(\bar{r}, p, t)}{\partial t} = Q(\bar{r}, p) + \nabla \cdot [D_{xx} \nabla \psi - \bar{V} \psi] + \frac{\partial}{\partial p} \left[ p^2 D_{pp} \frac{\partial \psi}{\partial p} \right] - \frac{\partial}{\partial p} \left[ \frac{dp}{dt} \psi - \frac{1}{3} p \nabla \cdot \bar{V} \psi \right] - \frac{\psi}{\tau_f} - \frac{\psi}{\tau_d}. \quad (1)$$

On the left side, we have the time variation of the  $\psi$  function that represents the density of particles per unit of momentum. On the right side, the first term ( $Q(\bar{r}, p)$ ) represents the sources of **CRs** such as **SNRs** or secondary production by nuclear interactions. The second term corresponds to the diffusion and convective part, where  $D_{xx}$  is the diffusion coefficient and  $V$  is the convection velocity. The third term refers to the diffusive reacceleration process, with a diffusion coefficient in the momentum space  $D_{pp}$ . The fourth term describes energy loss processes, in particular, momentum loss due to interactions with the **ISM** and losses due to non-uniform convection. Finally, the last two terms indicate losses by fragmentation or annihilation and losses by radioactive decay respectively.

To simulate the propagation process of  $\bar{d}$  in the Galaxy, the open source code GALPROP v. 5.7 [7] is used. GALPROP solves the transport equation numerically, and introduces current astrophysical models and data to make the simulation more realistic. For the present study, a two-dimensional diffusion halo with cylindrical symmetry is considered. The parameters on the transport equation (including the size of the Galaxy, and diffusion coefficient, among others), were set according to Boschini *et al.* [8].

## 52 3 Secondary antideuteron production

### 53 3.1 Coalescence model

54 The coalescence model postulates that an  $\bar{d}$  can be formed if an antiproton ( $\bar{p}$ ) and an antineutron ( $\bar{n}$ ) produced after an interaction are close in phase space within a volume determined  
55 by a radius in momentum  $p_0$  [9, 10], known as the coalescence momentum. In this way, a  
56 primary accelerated p or He, with enough energy, interacting with a p or He of the **ISM**, might  
57 produce a sequence of  $\bar{p}$  and  $\bar{n}$  that could coalesce to form  $\bar{d}$  or increasingly heavier antinuclei.

58 As a first analytical approach, the distribution of the  $\bar{p}$ - $\bar{n}$  pair momentum can be seen as  
59 the product of two independent isotropic distributions, without correlation [11]. In this way,  
60 the  $\bar{d}$  spectrum is given by  
61

$$\gamma_{\bar{d}} \frac{\partial^3 N_{\bar{d}}}{dp_{\bar{d}}^3} = \frac{4\pi}{3} p_0^3 \left( \gamma_{\bar{p}} \frac{\partial^3 N_{\bar{p}}}{dp_{\bar{p}}^3} \right) \left( \gamma_{\bar{n}} \frac{\partial^3 N_{\bar{n}}}{dp_{\bar{n}}^3} \right), \quad (2)$$

62 where  $\frac{\partial^3 N}{dp^3}$  represents the differential yield per event of particle ( $\bar{p}$ ,  $\bar{n}$  and  $\bar{d}$ ) in terms of momen-  
63 tum,  $\gamma$  is the Lorentz factor for each particle and  $p_0$  is the coalescence momentum. However,  
64 the production of antinuclei pairs in nuclear collisions is not independent or isotropic, i.e. they  
65 are correlated [12]. To take these correlations into account, the coalescence mechanism to  
66 form  $\bar{d}$  is simulated on an event-by-event basis, using  $\bar{p}$ - $\bar{n}$  pairs produced in p-p, p-He, He-p,  
67 and He-He collisions with Monte Carlo (**MC**) generators. Collisions simulated with **MC** gener-  
68 ators follow interaction models that already contain correlations between products [13]. To  
69 generate a new  $\bar{d}$  from any  $\bar{p}$ - $\bar{n}$  pair, the center of mass momentum of the pair  $p_{cm}$  should be  
70 less than the coalescence momentum, i.e.  $p_{cm} < p_0$ . The value of  $p_0$  is chosen in a way the  
71 final  $\bar{d}$  differential cross section is in agreement to accelerator measurements [14]. On the  
72 other hand, the condition on the  $\bar{p}$ - $\bar{n}$  pair separation boundary ( $\Delta x$ ) is enforced by allowing  
73 only  $\bar{d}$  that are generated within a radius of  $\sim 2fm$  to coalesce. Here, **CRs** collisions and  $\bar{d}$   
74 production simulated with EPOS-LHC generator and a coalescence afterburner by Shukla *et*  
75 *al.* [15] and Gomez-Coral *et al.* [12] were used.

### 76 3.2 Secondary source term

77 The secondary source term  $Q$  (see Eq. 1) for  $\bar{d}$  production by **CRs** collisions can be written as  
78 follows:

$$Q_{\bar{d}}^{sec}(E_{kin}^{\bar{d}}, \mathbf{r}) = \sum_{i \in \{p, He, \bar{p}\}} \sum_{j \in \{p, He\}} 4\pi n_j(\mathbf{r}) \int_{E_{kin}^{\bar{d}}}^{\infty} \frac{d\sigma_{i,j}(E_{kin(i)}, E_{kin}^{\bar{d}})}{dE_{kin}^{\bar{d}}} \Phi_i(E_{kin(i)}, \mathbf{r}) dE_{kin}, \quad (3)$$

79 where  $n_j$  is the particle density of the **ISM**,  $E_{kin(i)}$  denote the kinetic energy per nucleon of  
80 the incident particles,  $\Phi_i$  the incident flux of **CRs** (p and He) and  $\left( \frac{d\sigma_{prod}}{dE_{kin}^{\bar{d}}} \right)_{i,j}$  corresponds to  
81 the differential cross section for  $\bar{d}$  with  $E_{kin}^{\bar{d}}$  the kinetic energy per nucleon for  $\bar{d}$  [16]. The  
82 secondary source term convolves the  $\bar{d}$  differential production cross section obtained using  
83 EPOS-LHC and the coalescence model [17] (see Sec. 3.1).

84 **4 Results**85 **4.1 Differential cross section production and source term for  $\bar{d}$** 

86 From the limited discrete data generated with EPOS-LHC and the coalescence simulation of  
 87  $\bar{d}$  published by Shukla *et al* [15] (color points in Fig.1 (a)), a polynomial fit was performed  
 88 over a continuous interval of  $\bar{d}$  kinetic energy per nucleon, for every set of data points per  
 89 projectile kinetic energy (color lines in Fig.1 (a)). Then, the parameters obtained from this fit  
 90 were interpolated as a function of the projectile kinetic energy per nucleon, to get a complete  
 91 parametrization of the  $\bar{d}$  production cross sections.

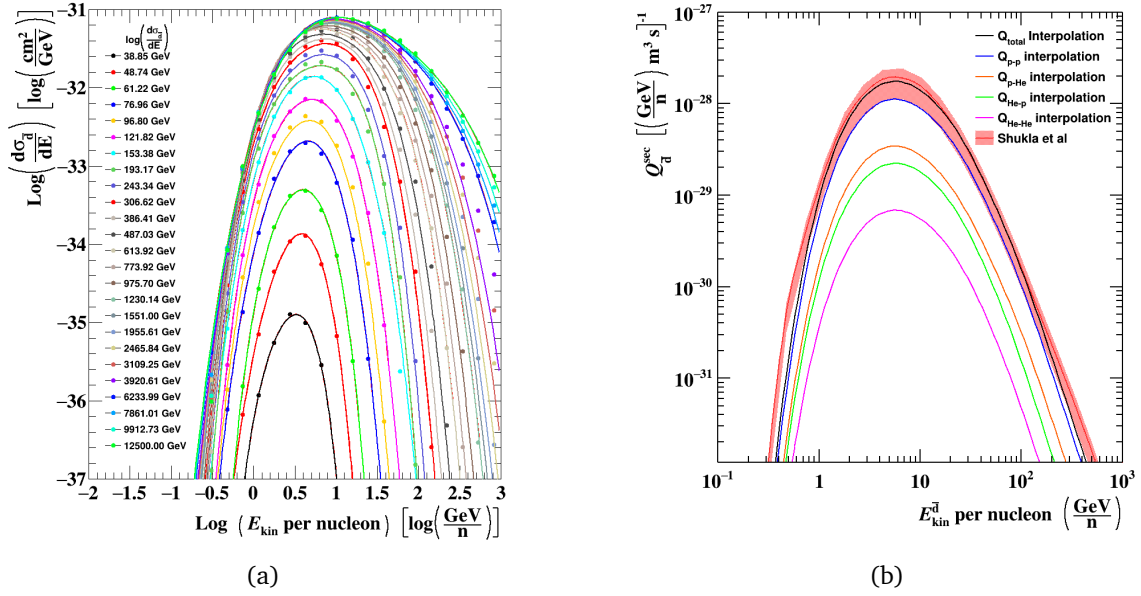


Figure 1: (a):  $\bar{d}$  production differential cross section ( $\frac{d\sigma_{\bar{d}}}{dE}$ ), as a function of  $\bar{d}$  kinetic energy per nucleon in log-log scale, for different projectile energies. (b): Total secondary  $\bar{d}$  source term (black line) and contributions from all types of CRs collisions (color lines) calculated with a parametrization function and compared to [15] (red band).

92 Then, the secondary source term was estimated using the  $\bar{d}$  production cross section parametriza-  
 93 tion in Eq. 3, and was compared to [15]. The results are shown in Fig. 1 (b), where can be  
 94 seen that both results (solid black line and red solid line) are in agreement for most of the  $\bar{d}$   
 95 energy range.

96 **4.2 Expected  $\bar{d}$  flux**

97 Finally, the  $\bar{d}$  production cross section parametrization was implemented in GALPROP v. 57  
 98 (Sec. 2) where  $\bar{d}$  were propagated using updated propagation parameters. Solar modulation  
 99 was modeled using the Force Field approximation [18].  $\phi_F$  was obtained from a fit of the  
 100 model to AMS-02  $\bar{p}$  measurements [19]. The resulting Top-Of-Atmosphere TOA fluxes as a  
 101 function of kinetic energy per nucleon for  $\bar{p}$  (blue solid line) and  $\bar{d}$  (red line) are shown in Fig. 2  
 102 along with AMS-02  $\bar{p}$  data [19] (black points) and AMS-02  $\bar{d}$  expected sensitivity [20] (green  
 103 lines). The red band in Fig. 2 represents the  $\bar{d}$  cross section uncertainty estimated in [15] as  
 104 35% above and 45% below the expected flux.

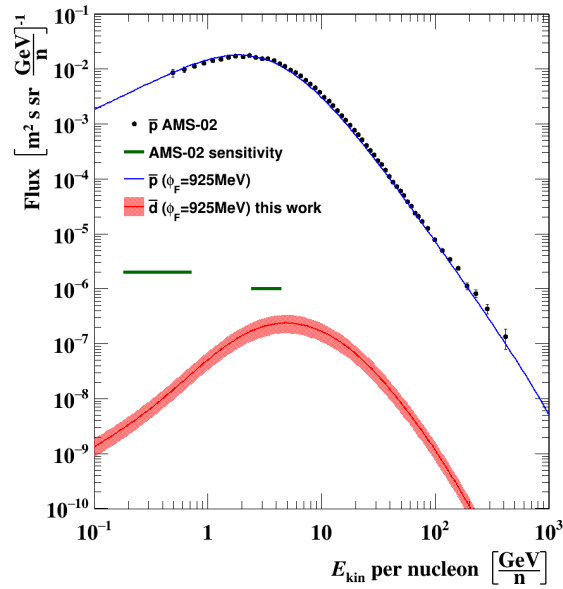


Figure 2: Estimated secondary  $\bar{d}$  flux with GALPROP v.57 (red line) and its uncertainties associated with cross sections (red band). For comparison, the  $\bar{d}$  AMS-02 expected sensitivity is shown as green lines [20]. The modulated  $\bar{p}$  flux calculated with GALPROP v.57 (blue line) is compared to  $\bar{p}$  AMS-02 data [19] (black points).

## 105 5 Conclusion

106 The expected secondary  $\bar{d}$  flux was estimated by performing a parametrization of the  $\bar{d}$  pro-  
 107 duction cross sections as a function of  $\bar{d}$  kinetic energy and projectile energy, using MC data  
 108 generated by [15]. To propagate  $\bar{d}$  in the Galaxy, GALPROP v.57 was used along with the  
 109 latest propagation parameters from [8]. The expected sensitivity of the AMS-02 experiment  
 110 reported in [20] was compared to the calculated  $\bar{d}$  flux, being above by a factor of 3 (Fig. 2).  
 111 This suggest the  $\bar{d}$  candidates reported by AMS-02 are not coming from a secondary origin.  
 112 However, measurements in  $\bar{d}$  production cross sections for projectile energies between 100 to  
 113 200 GeV are necessary to corroborate a coalescence momentum dependence with projectile  
 114 energy [12]. A significant different  $\bar{d}$  flux can be obtained by considering a constant  $p_0$  [21].

## 115 Acknowledgements

116 The authors thank Anirvan Shukla for sharing the MC-generated data. This work was sup-  
 117 ported by UNAM-PAPIIT IA101624 and by CONAHCYT under grant CBF2023-2024-118. LFGC  
 118 thanks the support from CONAHCYT-[CVU-937792] scholarship and PAEP-UNAM.

## 119 References

- 120 [1] C. Grupen, *Astroparticle Physics*, Springer International Publishing, ISBN 9783030273392,  
 121 doi:<https://doi.org/10.1007/978-3-030-27339-2> (2020).  
 122 [2] F. Donato, N. Fornengo and D. Maurin, *Antideuteron fluxes from dark matter annihilation in diffu-  
 123 sion models*, Physical Review D **78**(4) (2008), doi:[10.1103/PhysRevD.78.043506](https://doi.org/10.1103/PhysRevD.78.043506).

- 124 [3] P. v. Doetinchem *et al.*, *Cosmic-ray antinuclei as messengers of new physics: status and outlook*  
125 *for the new decade*, *Journal of Cosmology and Astroparticle Physics* **2020**(08), 035 (2020),  
126 doi:[10.1088/1475-7516/2020/08/035](https://doi.org/10.1088/1475-7516/2020/08/035).
- 127 [4] S. Ting, *Latest results from ams on the international space station* (2023).
- 128 [5] P. Blasi, *Charged particles in magnetic fields and cosmic ray transport* (2023),  
129 doi:[10.48550/arXiv.2307.11640](https://doi.org/10.48550/arXiv.2307.11640).
- 130 [6] L. Šerkšnytė *et al.*, *Reevaluation of the cosmic antideuteron flux from cosmic-ray interactions and*  
131 *from exotic sources*, *Physical Review D* **105**(8) (2022), doi:[10.1103/PhysRevD.105.083021](https://doi.org/10.1103/PhysRevD.105.083021).
- 132 [7] T. A. Porter, G. Jóhannesson and I. V. Moskalenko, *The galprop cosmic-ray propagation and non-*  
133 *thermal emissions framework: Release v57*, *The Astrophysical Journal Supplement Series* **262**(1),  
134 30 (2022), doi:[10.3847/1538-4365/ac80f6](https://doi.org/10.3847/1538-4365/ac80f6).
- 135 [8] M. J. Boschini *et al.*, *Inference of the local interstellar spectra of cosmic-ray nuclei  $z \leq 28$  with the*  
136 *galprop-helmod framework*, *The Astrophysical Journal Supplement Series* **250**(2), 27 (2020),  
137 doi:[10.3847/1538-4365/aba901](https://doi.org/10.3847/1538-4365/aba901).
- 138 [9] S. T. Butler and C. A. Pearson, *Deuterons from high-energy proton bombardment of matter*, *Physical*  
139 *Review* **129**(2), 836 (1963), doi:<https://doi.org/10.1103/PhysRev.129.836>.
- 140 [10] L. Csernai and J. I. Kapusta, *Entropy and cluster production in nuclear collisions*, *Physics Reports*  
141 **131**(4), 223 (1986), doi:[https://doi.org/10.1016/0370-1573\(86\)90031-1](https://doi.org/10.1016/0370-1573(86)90031-1).
- 142 [11] P. Chardonnet *et al.*, *The production of anti-matter in our galaxy*, *Physics Letters B* **409**(1–4), 313  
143 (1997), doi:[https://doi.org/10.1016/S0370-2693\(97\)00870-8](https://doi.org/10.1016/S0370-2693(97)00870-8).
- 144 [12] D.-M. Gomez-Coral, A. Menchaca Rocha, V. Grabski, A. Datta, P. von Doetinchem and A. Shukla,  
145 *Deuteron and antideuteron production simulation in cosmic-ray interactions*, *Physical Review D*  
146 **98**(2) (2018), doi:<https://doi.org/10.1103/PhysRevD.98.023012>.
- 147 [13] M. Kachelriess, I. V. Moskalenko and S. S. Ostapchenko, *New calculation of antiproton pro-*  
148 *duction by cosmic ray protons and nuclei*, *The Astrophysical Journal* **803**(2), 54 (2015),  
149 doi:[10.1088/0004-637X/803/2/54](https://doi.org/10.1088/0004-637X/803/2/54).
- 150 [14] B. Alper *et al.*, *Large angle production of stable particles heavier than the proton and a*  
151 *search for quarks at the cern intersecting storage rings*, *Physics Letters B* **46**(2), 265 (1973),  
152 doi:[https://doi.org/10.1016/0370-2693\(73\)90700-4](https://doi.org/10.1016/0370-2693(73)90700-4).
- 153 [15] A. Shukla, A. Datta, P. von Doetinchem, D.-M. Gomez-Coral and C. Kanitz, *Large-scale simu-*  
154 *lations of antihelium production in cosmic-ray interactions*, *Physical Review D* **102**(6) (2020),  
155 doi:<https://doi.org/10.1103/PhysRevD.102.063004>.
- 156 [16] A. Ibarra and S. Wild, *Determination of the cosmic antideuteron flux in a monte carlo approach*,  
157 *Physical Review D* **88**(2) (2013), doi:<http://dx.doi.org/10.1103/PhysRevD.88.023014>.
- 158 [17] D. Gomez Coral and A. Menchaca-Rocha, *Sm antideuteron background to indirect dark matter*  
159 *signals in galactic cosmic rays*, *Journal of Physics: Conference Series* **1602**(1), 012005 (2020),  
160 doi:[10.1088/1742-6596/1602/1/012005](https://doi.org/10.1088/1742-6596/1602/1/012005).
- 161 [18] L. J. Gleeson and W. I. Axford, *Solar modulation of galactic cosmic rays*, *The Astrophysical Journal*  
162 **154**, 1011 (1968), doi:[10.1086/149822](https://doi.org/10.1086/149822).
- 163 [19] M. Aguilar *et al.*, *The alpha magnetic spectrometer (ams) on the international space sta-*  
164 *tion: Part ii — results from the first seven years*, *Physics Reports* **894**, 1 (2021),  
165 doi:<https://doi.org/10.1016/j.physrep.2020.09.003>.
- 166 [20] T. Aramaki *et al.*, *Review of the theoretical and experimental status of dark mat-*  
167 *ter identification with cosmic-ray antideuterons*, *Physics Reports* **618**, 1 (2016),  
168 doi:<https://doi.org/10.1016/j.physrep.2016.01.002>.
- 169 [21] P. D. L. T. Luque, M. W. Winkler and T. Linden, *Cosmic-ray propagation models elucidate the prospects*  
170 *for antinuclei detection*, *Journal of Cosmology and Astroparticle Physics* **2024**(10), 017 (2024),  
171 doi:[10.1088/1475-7516/2024/10/017](https://doi.org/10.1088/1475-7516/2024/10/017).